RESEARCH ARTICLE

Strong adsorption of metolachlor by biochar prepared from walnut shells in water

Lu Liu[1] · Yingjie Dai[1]

Abstract

In this study, we investigated the removal of metolachlor (MET) by biochar (BC) prepared from walnut shells (W-BC) compared with BCs made from cow dung (D-BC) and corn cobs (C-BC) by characterizing the adsorption kinetics, pH, adsorbent dose, and ionic strength, and using isotherm models. Weight analysis was also conducted to understand the adsorption capacity and adsorption mechanisms. The results showed that the MET removal rates were 87.89% (W-BC), 52.91% (D-BC), and 10.91% (C-BC), respectively. According to the results fitted to the Langmuir isotherm model, the saturated adsorption capacities for MET were 96.15 mg g^{-1}, 37.88 mg g^{-1}, and 11.98 mg g^{-1} with W-BC, D-BC, and C-BC, respectively. The results demonstrated that W-BC was particularly effective at MET removal. Analyses based on the weights of different factors showed that the correlation coefficient was highest for the BC type with 46.11% in the MET adsorption process, followed by the initial concentration of MET (19.29%). The adsorption of MET by BCs was probably influenced mostly by electron donor–acceptor interactions and pore filling. These results may facilitate further studies of the adsorption mechanism and optimization of the process.

Keywords Adsorbent · BC · Kinetics · Pyrolysis · Water pollution

Introduction

In order to meet the food requirements of the growing global population, the use of herbicides to control weeds has become a key component of large-scale agricultural production (Rose et al. 2018). Metolachlor (MET) is an amide herbicide used mainly to kill broadleaf grass in the pre-emergent stage (Deng et al. 2020). MET prevents root and bud elongation by inhibiting glutathione (Rytow et al. 2008). The low cost of MET explains why it is the fourth most widely used selective herbicide throughout the world, and it accounts for 4.2% of global herbicide use (Rose et al. 2018). As a consequence, MET is one of the most common herbicides found in water samples from agricultural areas in the USA. Similar to atrazine and deethylatrazine, MET and its metabolites have been found widely in surface and groundwater in the USA, and even in remote lakes (Rose et al. 2018). The annual usage of MET is the highest among amide herbicides, and it is applied widely for selective weed control in various field crops in China (Wei et al. 2016). Due to its solubility in water (530 mg L^{-1} at 20 °C) and long half-life (120 days), the damage caused to aquatic ecosystems by MET has become a global environmental issue (Josef et al. 2018). MET is a potential human carcinogen with moderate to high chronic toxicity, and some of its metabolites such as 2-ethyl-6-methylamine are highly toxic (Barra et al. 2005). In 1993, the World Health Organization listed MET as a human carcinogen, and the US Environmental Protection Agency also classified it as a category C carcinogen (Sun et al. 2019). MET can directly affect immune organs or cells, cause damage to the body's immune system, and reduce the body's capacity to resist infections and eliminate tumor cells (Hu 2009). Therefore, the usage of large amounts of MET with high cytotoxicity and genetic toxicity poses a threat to human health.

In recent years, the methods employed for removing MET from water environments include biodegradation (Sun et al. 2019), photodegradation (Wu et al. 2007), advanced oxidation (Orge et al. 2017), membrane (Tijani et al. 2017), electrochemical (Guelfi et al. 2018), and adsorption (Dai et al. 2020). Compared with other methods, adsorption is safer

and simpler to operate, with no secondary pollution, a high economic feasibility, and a high removal efficiency. Many different types of adsorbents are available, such as particulate carbon (Kumar et al. 2017), nanotubes (Zhong et al. 2017), polymer resins (Vinhal et al. 2016), and mineral materials (Shattar et al. 2019). Some of these materials have been employed to remove MET from wastewater but high costs limit their use. Therefore, it is necessary to develop environmentally friendly materials with low costs and a high capacity for removing MET (Mandal et al. 2017).

Biomass has become an important renewable resource and its utilization has received increasing attention (Stapf 2017). Biochar (BC) is the main product of biomass pyrolysis under oxygen-limited conditions (Kan et al. 2016). BCs were first used as soil improvers, but their porous structures have attracted much attention in recent years because of the potential application of BCs as adsorbents in water (Dai et al. 2019a, 2019b; Nguyen et al. 2017). Compared with many adsorbents, BCs are inexpensive and they can be produced from various types of raw materials, and they are readily recycled. Thus, environmentally friendly BCs potentially have economic benefits and broad application prospects in the treatment of polluted water (Chen et al. 2017). In a previous study, rice straw was subjected to low-temperature oxygen-limited pyrolysis to produce BC for adsorbing MET (Ge et al. 2016). However, the specific surface area was low (2.56 m^2 g^{-1}) for BC carbonized at a low temperature (200 °C) and the pores were underdeveloped in this material (Wei et al. 2016). In another study, rice husk BC was used to adsorb MET and its adsorption capacity was determined. The adsorption performance of the high-temperature BC (750 °C) was analyzed, but the reproducibility of adsorption by the BC was not tested, and the effects of the pH and ionic strength were not considered. Therefore, it is not possible to provide reliable recommendations regarding the actual adsorption of MET using this material. Cwielag-Piasecka et al. (2018) used wheat straw to produce BC and adsorb MET, but the effects of environmental factors such as pH were not analyzed (Cwielag-Piasecka et al. 2018). The main types of BCs are straw BC, manure BC, wood BC, sludge BC, and shell BC (Yuan et al. 2016). The research on straw BC and manure BC is more common (He et al. 2020; Xu et al. 2020; Zhang et al. 2019; Zhang et al. 2020). There are few studies on shell BC, so the research on shell BC is urgently needed. Moreover, no analyses were conducted of various factors and the contribution of each factor to the adsorption capacity, which would be useful for optimizing the adsorption conditions. Several studies have shown that BCs produced from different types of biomass can be used to remove MET, but previous investigations did not comprehensively assess the adsorption of MET using BCs prepared from walnut shells, cow dung, and corn cobs.

The potential application of specific types of BC for the adsorption of pollutants depends greatly on their inherent physical and chemical properties (Ozcimen and Ersoy-Mericboyu 2010).

The properties of BCs are first affected by the properties of the original materials (Wei et al. 2017). Therefore, we hypothesized that during the adsorption of MET on BCs, the characteristics of the BCs (such as the specific surface area, pore volume, and pore diameter) will have the most critical effects on adsorption.

In this study, we analyzed the surface structures of three BCs by scanning electron microscopy and the crystal structures by X-ray diffraction. Brunauer–Emmett–Teller analysis (BET) was used to determine the specific surface area (S_{BET}), porosity, and pore volume of the BCs. Fourier transform infrared spectroscopy was applied to analyze the functional groups on the surfaces and the bonds in the BCs. The MET adsorption behavior and mechanism were also determined for the BCs. We analyzed each factor and compared their contributions to the adsorption process in order to optimize the adsorption conditions. Weight analysis was performed based on correlations in order to analyze and evaluate the quality of the three BCs by determining the critical factors that affected their adsorption capacity.

Materials and methods

Materials and chemicals

MET (C$_{15}$H$_{22}$ClNO$_2$, purity > 97.0%) was obtained from Shuzhou Xianzhengda Co. Ltd, China. The detailed physical and chemical properties of MET are shown in Table 1. All reagents were analytically pure chemicals. MET was formulated at different concentrations in deionized water and distilled water. Walnut shells were obtained from Northeast Pecans of China; cow dung was collected from Xiangfang livestock farm in Harbin, China; and corn cobs were acquired from an experimental field at Northeast Agricultural University in Harbin, China. The raw materials were washed with distilled water, dried in an oven for 48 h, and ground into small pieces, before heating to 700 °C in a programmable muffle furnace at a heating rate of 5 °C min^{-1}, and carbonization was continued for 2 h. After cooling, the samples were removed from the muffle furnace, washed, and ground until they passed through a 100-mesh screen. W-BC prepared from walnut shells, D-BC from cow dung, and C-BC from corn cobs were obtained by using the same preparation method.

Physical and chemical characteristics of BCs

A scanning electron microscope (S-3400N, Tokyo Hitachi Co. Ltd., Japan) was used to analyze the surface structures of the W-BC, D-BC, and C-BC samples, and energy dispersive X-ray (EDS) spectra were also obtained. BET analysis was conducted to determine the specific surface areas of the BCs with an elemental analyzer (CHN CORDER MT-6, Yanagimoto Co. Ltd., Japan). After drying a small amount of the BC particles overnight and degassing under nitrogen protection, the N$_2$ adsorption

isotherms were measured in a N_2 bath (-196 °C). The specific surface areas were calculated for W-BC, D-BC, and C-BC using the BET formula. The physical adsorption of nitrogen by a gas absorber was used to obtain the pore parameters for BET analysis. An X'Pert PRO diffractometer (D8 Advance, Bruker, Germany) was used to obtain diffraction patterns. Fourier transform infrared spectroscopy (Nicolet FTIR 6700, USA) was conducted to identify the surface functional groups on the BCs. Elemental analysis was performed for W-BC, D-BC, and C-BC with a MICRO CORDER JM10 (J-Science Lab Co. Ltd., Kyoto, Japan).

Adsorption experiments

The effects of the contact time, initial concentration (C_0), BC dose, initial pH, ionic strength, and regeneration on the adsorption performance were investigated, and the kinetics and isotherms were analyzed. First, 25 mL of MET solution was added to a 50-mL beaker containing a fixed amount of BC, before oscillating in a shaker at 150 rpm and a constant temperature for a specific period of time (5 min to 7 h). The supernatant was filtered through a 0.45-μm filter membrane, and the absorbance was measured at 235 nm with an ultraviolet spectrophotometer (UV-1800, Shimadzu, Tokyo, Japan). The corresponding MET concentrations based on different absorbances were calculated using a previously prepared standard working curve. The pH of each solution was adjusted from 3.0 to 13.0 as required with 0.1 mol L^{-1} HCl and 0.1 mol L^{-1} NaOH. The adsorbent dosage varied among 0.12–0.80 g L^{-1}. C_0 for MET was 5–30 mg L^{-1}, and the adsorption temperature was maintained at 25 °C. A blank control containing only MET and no added BC was included in each experiment. Each group of experiments was repeated three times, and the average was calculated based on three replicates.

Before the regeneration experiment was performed, BCs containing MET soaked in deionized water were desorbed three times at 10 kHz for 10 min each time to desorb, before washing the desorbed BCs with deionized water. The BC regeneration tests were then performed, and the analyses described above were repeated.

Data analysis

Adsorption kinetics studies

The adsorption kinetic models (pseudo-first-order and pseudo-second-order) are used to describe the kinetic mechanism of the adsorption process on the BC surface. The kinetic rate equation is as follows:

$$\frac{dq_t}{dt} = (q_e - q_t)^n \tag{1}$$

In Eq. (1), q_e (mg/g) represents the saturated adsorption scale, that is, the adsorption capacity at equilibrium, and q_t (mg/g) represents the MET adsorption capacity at time t. k_n is the rate constant for the nth-order adsorption (k_n units are 1/min for $n = 1$ and g/mg min for $n = 2$). The linear integral form of the equation is as follows:

First-order kinetics ($n = 1$):

$$\ln(q_e - q_t) = \ln q_e - k_1 t \tag{2}$$

Second-order kinetics ($n = 2$):

$$\frac{t}{q_t} = \frac{1}{k_2 q_e^2} + \frac{t}{q_e} \tag{3}$$

Based on the plots of $\ln(q_e - q_t)$ and t/q_t as a function of t, the first-order and second-order kinetic models and their rate constants (k_n) and correlation coefficients (R^2) can be determined. By linear regression, the values of the fitted equations, q_e, and R^2 are determined.

Adsorption isotherm

The Langmuir (Eq. (4)) and Freundlich (Eq. (5)) models are used to fit the adsorption process. The formula is as follows:

$$q_e = \frac{Q_0 K_L C_e}{1 + K_L C_e} \tag{4}$$

$$q_e = K_F C_e^{\frac{1}{n}} \tag{5}$$

Equation (4) is the Langmuir isotherm model. Among them, Q_0 (mg/g) represents the maximum adsorption capacity; C_e (mg/L) is the equilibrium concentration; and K_L (L/mg) represents the adsorption equilibrium constant of the Langmuir isotherm. Equation (5) is the Freundlich isotherm model. K_F (L/mg) is the affinity coefficient of the Freundlich isotherm; n, as a constant and an empirical parameter, is relevant to the adsorption strength of the adsorbent.

The weight of different factors on adsorption capacity

Data standardization Assume n and p are the number of samples and indicators. In the data standardization process, the positive indicators and the negative indicators can be standardized separately, and also, the indicators can be turned into the same trend first.

In this paper, the positive and negative indicators are standardized respectively by formula (6) and (7) (Rode 2019; Szabo 2015; Yu et al. 2009).

The positive indicators:

$$s_{ij} = \frac{x_{ij} - \min(x_j)}{\max(x_j) - \min(x_j)} \quad (i = 1, 2, ..., n; j = 1, 2, ..., p) \tag{6}$$

The negative indicators:

$$s_{ij} = \frac{\max(x_j) - x_{ij}}{\max(x_j) - \min(x_j)} \quad (i = 1, 2, \ldots, n; j = 1, 2, \ldots, p) \quad (7)$$

Weighting method of different indicators (factors) Due to the correlation between the indicators, the weight coefficient can be determined according to the internal dependent structure of the correlation matrix of all indicators (Dai et al. 2020).

Step 1: Calculate the correlation matrix $R = (r_{ij})_{pxp}$ of the standardized data matrix $S = (s_{ij})_{nxp}$.

Step 2: Calculate the mean value of the correlation coefficient between x_j and other indicators by formula (8):

$$\delta_j = \frac{\sum\limits_{1 \neq j}^{p} r_{ij}}{p-1} \quad (i = 1, 2, \ldots, p) \quad (8)$$

Step 3: Reverse the average correlation degree:

$$\alpha_j = \frac{\max_j \delta_j}{\delta_j} \quad (\alpha_j \geq 1, j = 1, 2, \cdots, p) \quad (9)$$

Step 4: Calculate the weight coefficient of x_j:

$$W_j = \frac{\alpha_j}{\sum\limits_{j=1}^{n} \alpha_j} \quad (j = 1, 2, \ldots, p) \quad (10)$$

The Pearson correlation coefficient and correlation matrix The Pearson correlation coefficient measures a linear dependence between two variables, and it is the most commonly used method in the correlation test.

The Pearson correlation coefficient calculated by formula (13):

$$r = \rho_{X,Y} = \frac{\text{cov}(X, Y)}{\sigma_X \sigma_Y} = \frac{E[(X - \mu x)(Y - \mu y)]}{\sigma_X \sigma_Y}$$
$$= \frac{\sum (x - E(X))(y - E(Y))}{\sqrt{\sum (x - E(X))^2 \sum (y - E(Y))^2}} \quad (11)$$

cov(X, Y) is the covariance, which can be calculated by formula (14):

$$\begin{aligned} Cov(X, Y) &= E[(X - E[X]) (Y - E[Y])] \\ &= E[XY] - 2E[X] E[Y] + E[X] E[Y] \\ &= E[XY] - E[X] E[Y] \end{aligned} \quad (12)$$

$E[X]$ (or $E[Y]$) is the mean value.

The corresponding linear correlation matrix can be obtained by calculating the Pearson correlation coefficient between each indicator.

Results and discussion

Physical and chemical characteristics of BCs

The pore structures on the surfaces of the BCs were observed by scanning electron microscopy. As shown in Fig. 1a, the surface of W-BC mainly comprised complex network structures. The surfaces of these networks were very rough with many adsorption sites to promote high adsorption. The surface of D-BC mainly comprised wrinkled and stacked structures, and the pore structures were not evenly distributed. These pores formed a complex network of connections on the surface of D-BC. Many irregular convex structures were present on the rough surface of C-BC. The pore structures were not obvious on the surface of C-BC, and the pores were not fully opened. EDS analysis of the three samples showed that the BCs contained Ca in addition to the common elements C and O. EDS analysis also showed that P was more evident on W-BC and D-BC. These elements were relatively more abundant on D-BC compared with the other two BC types.
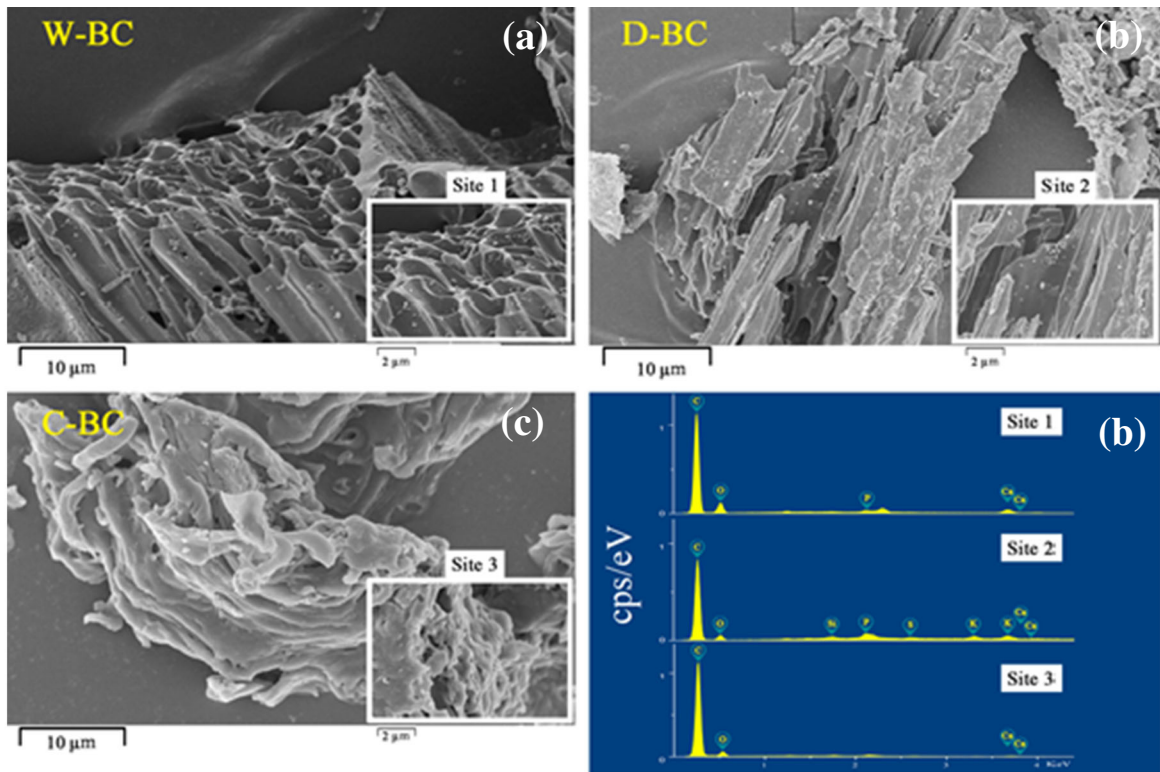
The specific surface areas of the BCs are shown in Table 2. The specific surface areas of W-BC, D-BC, and C-BC were determined as 358.67 m² g⁻¹, 141.72 m² g⁻¹, and 9.96 m² g⁻¹, respectively. Among the three types of BCs, W-BC had the largest pore volume (0.22 cm³ g⁻¹) and the smallest average pore size (1.9 nm). The total pore volumes determined for D-BC and C-BC were 0.09 cm³ g⁻¹ and 0.02 cm³ g⁻¹, respectively, and the average pore sizes were 6.55 nm and 13.46 nm. The X-ray diffraction intensity diagrams obtained for W-BC, D-BC, and C-BC are shown in Fig. 1b. In the pattern obtained for W-BC, the main peak intensity was found at $2\theta = 23.3°$. The main peaks for D-BC and C-BC were located at $2\theta = 22.9°$ and $2\theta = 23.5°$, respectively. The peak values between $2\theta = 16°$ and $2\theta = 30°$ indicate that BC deformed into graphene-like atomic structures due to pyrolysis at 700 °C.

As shown in Fig. 1c, the vibration absorption peak obtained for the three BCs at 3440 cm⁻¹ was the stretching vibration peak for –OH and the peak at 2922 cm⁻¹ was the vibration absorption peak for the hydrocarbon –CH₂ bond. In addition, the peak at 2350 cm⁻¹ was related to the nitrile (–C ≡ N) vibration, while that at 1630 cm⁻¹ was the stretching vibration
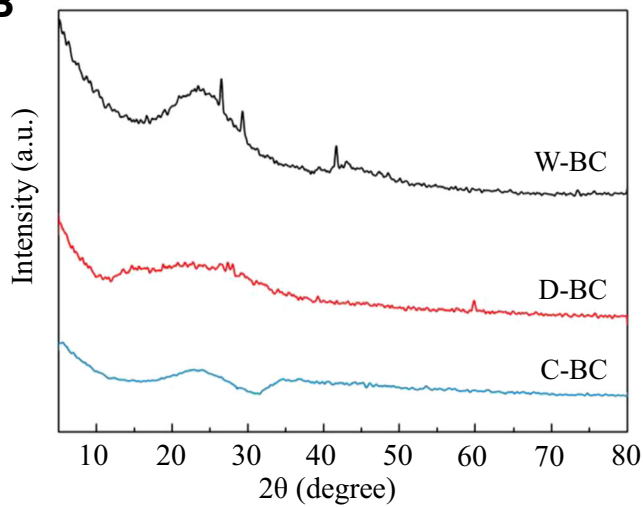
Fig. 1 **a** SEM/EDX analysis of BCs: (a) SEM image of W-BC; (b) SEM image of D-BC; (c) SEM image of C-BC; and (d) EDX spectrum of region inside image. **b** XRD patterns obtained for the W-BC, D-BC, and C-BC. **c** FTIR spectra obtained for the W-BC, D-BC, and C-BC
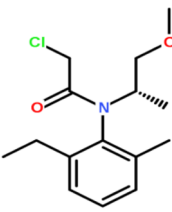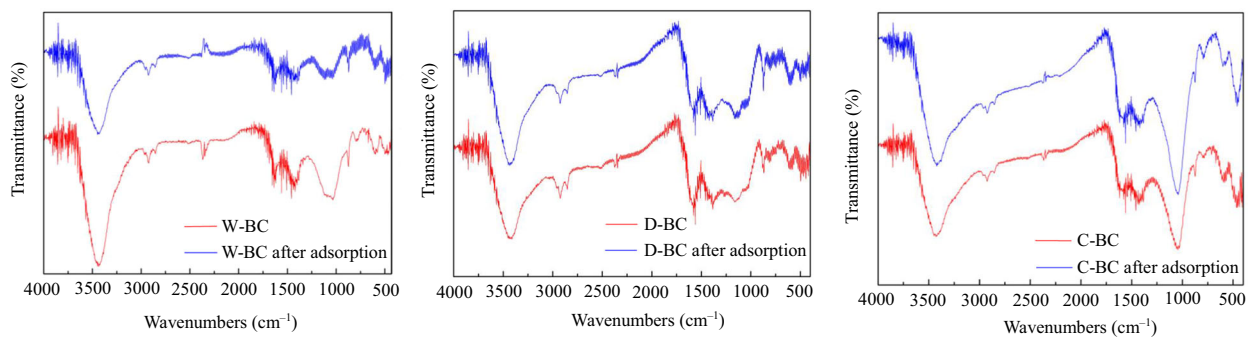
Table 1 Chemical structure and properties of MET

Chemical structure	
Chemical formula	$C_{15}H_{22}ClNO_2$
Molar mass (g mol^{-1})	283.5
Solubility in water (mg L^{-1}, 20 °C)	530
λ_{max} (nm)	235

of the double bond in aromatics (C=C), that at 1560 cm^{-1} was attributable to the –NH double bond or C–C double bond, the peak at 1420 cm^{-1} was due to alcohol hydroxyl or –COO, that at 1050 cm^{-1} was related to the vibration of –COR in aliphatic ethers, and the absorption peak at 600–900 cm^{-1} was mainly attributed to aromatic structures. According to Fig. 1c, all of the samples contained aromatic and heterocyclic structures, where C-BC was rich in free hydroxylic groups and aliphatic hydrocarbons on the surface, D-BC was rich in anhydrides, and W-BC had many oxygen-containing functional groups on the surface. The –OH absorption peaks obtained for C-BC before and after adsorption changed from 3410.58 to 3434.41 cm^{-1}, and the peak intensity changed little, whereas the intensities of the aromatic ring and aliphatic hydrocarbon absorption peaks decreased to some extent. Therefore, we suggest that π–π interactions occurred between MET and the π electrons provided by the oxygen-containing functional groups and aromatic compounds in C-BC, but hydrogen bonding had less effect. After MET was adsorbed by D-BC,

the intensity of the –OH vibration peak decreased and it moved from 3430.46 to 3421.45 cm^{-1}, while the average peak intensities at 1458 cm^{-1} and 400–900 cm^{-1} also decreased, which were due to the interactions among –OH hydrogen bonds and π–π bonds during the adsorption of MET by D-BC. Therefore, we consider that hydrogen bonding by –OH bonds and π–π bonds occurred during the adsorption of MET by D-BC. After the adsorption of MET by W-BC, the absorption peak at 2345 cm^{-1} disappeared and a new absorption peak appeared at 497.32 cm^{-1}, which was assigned to ketoyl vibration. The –CO absorption peak moved from 1033.12 to 1120.84 cm^{-1} and the intensity weakened. We inferred that the chemical bonds in the adsorption process underwent breakage and recombination. The main mechanism associated with the adsorption of MET by W-BC was related to π electrons, with less hydrogen bonding.

Adsorption kinetics

An important parameter when designing an adsorbent is the saturation of the adsorption time. Different adsorption equilibrium times will be associated with different adsorption rates (Treviño-Cordero et al. 2013). The removal rate is affected by the pore structure of the adsorbent, the amount of adsorbent, the C_0 values of pollutants, and the pH of the environment. Adsorbents with slower adsorption rates are not suitable for practical applications (Dai et al. 2019a, 2019b). The effects of the contact time on the adsorption of MET by the three BCs are shown in Fig. 2a. At the beginning of the adsorption process, the mass concentration of MET was higher in the solution and many adsorption sites were available on the BCs, so the adsorption rate was rapid. As the adsorption process continued, the concentration of MET in solution and the available adsorption sites decreased gradually. This effect was also demonstrated in previous studies that used BCs to remove MET (Ge et al. 2016; Liu et al. 2019). As shown in Fig. 2a, W-BC reached an equilibrium state after adsorption for 30 min and the removal rate was 98.3%. However, the removal rates with D-BC and C-BC were still low after 30 min. The adsorption equilibrium was only reached after 6 h with D-BC and C-BC, and the removal rates were 52.9% and 10.9%, respectively, which were far lower than that with W-BC.

Table 2 Physical and chemical properties of the samples

Sample	Yield (%)	S_{BET} (m^2 g^{-1})	Total pore volume (cm^3 g^{-1})	Average pore diameter (nm)	w (%)				Mass ratio		
					C	H	O	N	H/C	O/C	(N + O)/C
W-BC	40.93	358.67	0.22	1.90	82.53	2.03	8.51	0.83	0.295	0.077	0.086
D-BC	38.34	141.72	0.09	6.55	59.87	5.05	5.73	1.12	1.012	0.072	0.088
C-BC	46.89	9.96	0.02	13.46	78.46	4.03	7.84	3.02	0.616	0.075	0.108
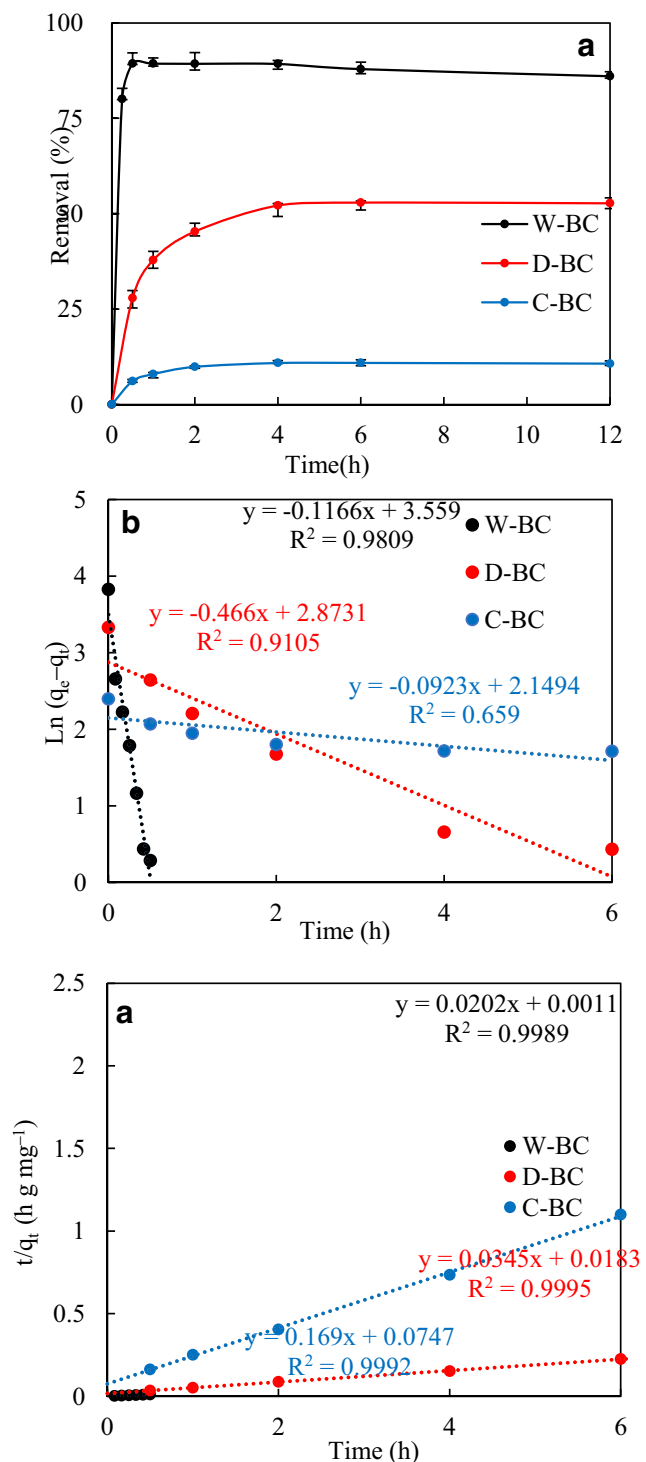
Fig. 2 **a** Effect of adsorption time by three BCs (C_0 of MET (10.00 mg L^{-1}), adsorbent dose = 0.20 g L^{-1}, pH 7.0, at 25 °C); **b** pseudo-first-order kinetic images of MET adsorption on three BCs; and **c** pseudo-second-order kinetic images of MET adsorption on three BCs (C_0 of MET (10.00 mg L^{-1}), adsorbent dose = 0.20 g L^{-1}, pH 7.0, at 25 °C)

In order to better describe the adsorption kinetics, we fitted adsorption kinetic models to the data. The fitted results for the pseudo-first-order and pseudo-second-order kinetic models

are shown in Figs. 2 and 3, respectively. The parameters are shown in Table 3. According to Table 3, the R^2 value was higher for the pseudo-second-order kinetic model than the pseudo-first-order kinetic model, and that for the pseudo-second-order kinetic model was higher than 99.8%. According to the pseudo-second-order kinetic model, the q_e values for W-BC, D-BC, and C-BC were 49.51 mg g^{-1}, 28.99 mg g^{-1}, and 5.92 mg g^{-1}, respectively, which agree well with the experimental adsorption capacities of 44.67 mg g^{-1}, 26.46 mg g^{-1}, and 5.46 mg g^{-1}. Thus, the adsorption process matched well with the pseudo-second-order kinetic model. The two kinetic models showed that both physical adsorption and chemical adsorption occurred in the adsorption process, but chemical adsorption was the main adsorption mechanism. The experimental and kinetic model data showed that compared with the other two types of BC, W-BC had a faster adsorption time and greater adsorption capacity.

Effects of BC doses

Figure 3a shows the adsorption of MET with different doses of BCs. As the adsorbent dose increased, the adsorption rate remained unchanged after adding a certain amount. The removal rate of MET by W-BC increased from 75.42 to 89.85% as the BC dosage increased from 0.12 to 0.80 g L^{-1}. The MET removal rates by D-BC and C-BC ranged from 38.23 to 60.40% and from 6.38 to 15.43%, respectively. The MET removal rate gradually increased as the BC dose increased because the BC provided more available adsorption sites, and more MET entered the pores on the surface of the BC. When the W-BC dose exceeded 0.20 g L^{-1}, the increase in the adsorption rate gradually decreased. Therefore, the BC dose used in the subsequent experiments was set to 0.20 g L^{-1} in order to improve the experimental efficiency.

Effects of pH

The changes in the MET removal rates by the three BCs at pH 3.0 to 13.0 are shown in Fig. 3b. The adsorption rate was higher when the pH was lower. The adsorption of MET by the BCs varied according to the pH. At pH = 3.0, the removal rates by W-BC, D-BC, and C-BC were 92.18%, 64.31%, and 13.50%, respectively. At pH 3.0–7.0, the MET removal rate decreased slightly as the pH increased. However, the removal rates by the three BCs were significantly reduced at pH 7.0–13.0. The inhibition of MET adsorption was more obvious when the pH was higher. At pH = 13.0, the removal rates by W-BC, D-BC, and C-BC were 27.26%, 12.41%, and 1.484%, respectively. Considering the natural degradation of MET in water, the removal rate with C-BC was extremely low under alkaline conditions, as also shown in previous studies of MET removal (Otero et al. 2016a; Shattar et al. 2019). Therefore, two main factors affected the adsorption of MET at different

Table 3   Parameters in pseudo-first-order and pseudo-second-order kinetic models of MET adsorption by BCs

Samples	Pseudo-first-order model			Pseudo-second-order model			
	$q_{e,\,cal}$ (mg g^{-1})	k_1 (h^{-1})	R^2	$q_{e,\,cal}$ (mg g^{-1})	k_2 (g mg^{-1} h)	R^2	$q_{e,expsss}$ (mg g^{-1})
W-BC	35.13	0.117	0.9808	49.51	0.0202	0.9989	44.67
D-BC	17.69	0.466	0.9150	28.99	0.0345	0.9995	26.46
C-BC	2.73	0.092	0.6590	5.92	0.1690	0.9992	5.46

pH values. First, the carbonyl and hydroxyl groups on the surfaces of the BCs were hydrolyzed as the pH increased, so the number of groups available to form hydrogen bonds with MET was reduced, thereby decreasing the MET removal rate (Otero et al. 2016a). Second, under acidic conditions, the electron-withdrawing groups connected to the aromatic ring on the BCs were protonated, thereby increasing the π-acceptors on the BCs, and the π–π electron interactions between BCs and MET enhanced the adsorption of MET. Thus, hydrogen bonds and π–π interactions were the main mechanisms responsible for the adsorption of MET by the BCs (Shattar et al. 2019).
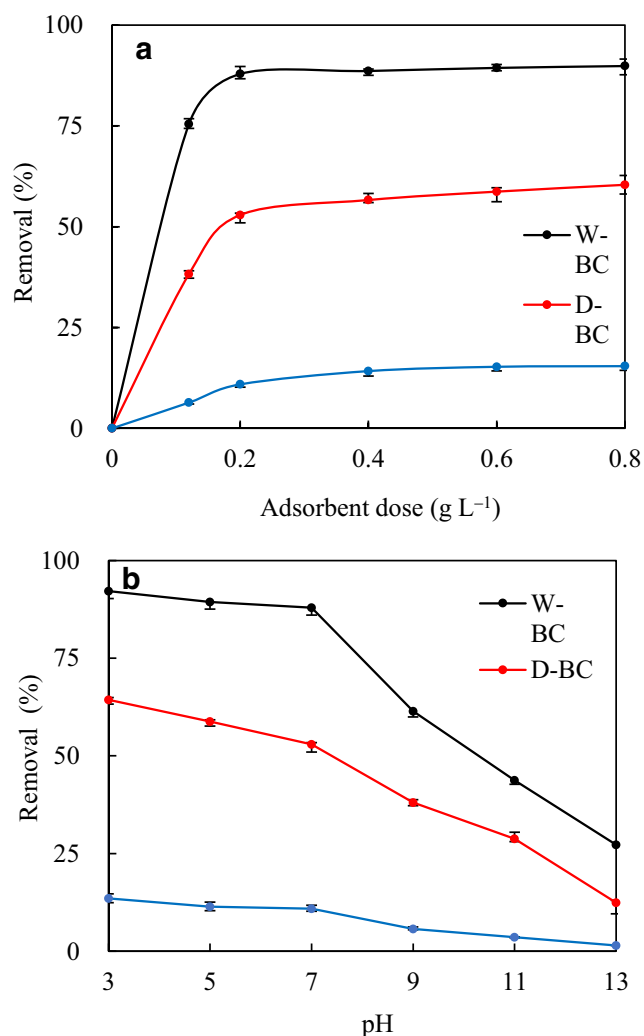
Adsorption isotherms

Figure 4 shows the adsorption isotherms obtained for the three BCs. The relevant parameters are summarized in Table 4. Langmuir and Freundlich isotherm models were employed for the analysis. The correlation coefficients (R^2) obtained for the BCs were higher with the Langmuir model than the Freundlich model, and thus, the results showed that the Langmuir model was more suitable. The Langmuir model describes the adsorption process of a single layer of adsorbent on a uniform surface. The saturated adsorption capacity (Q_0) values calculated for W-BC, D-BC, and C-BC using the Langmuir model were obtained as 96.15 mg g^{-1}, 37.88 mg g^{-1}, and 11.98 mg g^{-1}, respectively. The parameter obtained using the Freundlich isotherm model, i.e., $1/n$, was less than 1.000, thereby indicating that the adsorbent had a positive effect on the adsorption process.

Table 5 shows the Q_0 values obtained for different adsorbents with MET in previous studies and those obtained for the BCs examined in the present study. The Q_0 value obtained for W-BC in the present study is better than those determined for other adsorbents, such as rice straw BC (29.97 mg g^{-1}) (Ge et al. 2016), natural organic matter (3.90 mg g^{-1}) (Sigmund et al. 2019), montmorillonite (84.75 mg g^{-1}) (Qu al. 2020), and medium microporous silicone (55.03 mg g^{-1}) (Otero et al. 2016b). The values compared in Table 5 indicate that W-BC has a high saturation adsorption capacity for MET.

Effects of ionic strength

In actual wastewater, the presence of metal ions and their counter ions will increase the ionic strength, which may affect the MET adsorption performance. Therefore, Na$^+$, in aqueous solution with pH = 7, was used to evaluate the potential

Fig. 3   a Effect of adsorbent dose for the MET adsorption on three BCs (C_0 of MET (10.00 mg/L), shaking time 6 h, pH 7.0, at 25 °C) and **b** effect of pH on the adsorption of MET on three BCs (C_0 of MET (10.00 mg L^{-1}), adsorbent dose = 0.20 g L^{-1}, at 25 °C)

Table 4 Parameters for MET adsorption isotherms fitted with Langmuir and Freundlich models

Samples	Langmuir model			Freundlich model		
	Q_0 (mg g^{-1})	K_L (L mg^{-1})	R^2	K_F (L mg^{-1})	$1/n$	R^2
W-BC	96.15	0.7170	0.9781	43.46	0.3098	0.9691
D-BC	37.88	0.4550	0.9964	15.33	0.2794	0.9168
C-BC	11.98	0.0960	0.9946	1.52	0.5661	0.9943

adsorption of MET by BCs in an aqueous solution, and the results are shown in Fig. 5a. When the Na$^+$ concentrations were 0, 0.01 mol L^{-1}, 0.05 mol L^{-1}, and 0.1 mol L^{-1}, the MET removal rates with W-BC were 87.89%, 90.37%, 93.82%, and 91.24%, respectively; the removal rates with D-BC were 52.91%, 64.01%, 62.54%, and 60.31%; and the removal rates with C-BC were 10.91%, 15.30%, 14.71%, and 12.20%. Thus, the MET removal rates with the BCs exhibited a similar trend. The removal rates were highest with C-BC and D-BC when the Na$^+$ concentration was 0.01 mol L^{-1}. The highest MET removal rate was obtained with W-BC when the Na$^+$ concentration was 0.05 mol L^{-1}. At a Na$^+$ concentration of 0.1 mol L^{-1}, the MET adsorption rates by the three BCs were slightly lower compared with those at concentrations of 0.05 mol L^{-1}. This trend is similar to those obtained in other studies (Yang et al. 2014). The MET adsorption capacity in the concentration range of 0–0.05 mol L^{-1} increased with the ionic strength of Na$^+$, although the increase was gradual. The following two effects might explain this adsorption process. First, the increase in the ionic strength may have enhanced the hydrophobicity of MET and decreased its solubility, thereby resulting in a salting-out effect (Yang et al. 2014). Second, Na$^+$ may have penetrated the surfaces of the BCs to reduce the repulsion effect and tight aggregate structures may have formed between the BCs. When the Na$^+$ concentration was 0.05 mol L^{-1}, the MET removal rate increased significantly, thereby indicating that salting-out competition occurred between Cl$^-$ and MET on the surfaces of the BCs to enhance the adsorption of MET. However, when the Na$^+$ concentration was greater than 0.05 mol L^{-1}, the MET removal rate increased relatively slowly and a squeezing effect may have limited the adsorption of MET (Li et al. 2018).

Regeneration capacities

In order to assess the reusability of the BCs, the MET attached to the pores on the surfaces of BCs was desorbed by ultrasonic vibration after the adsorption experiment. The results obtained in the regeneration experiments are shown in Fig. 5b. After two cycles, the removal rates with W-BC, D-BC, and C-BC decreased by 48.42%, 32.20%, and 7.77%, respectively.
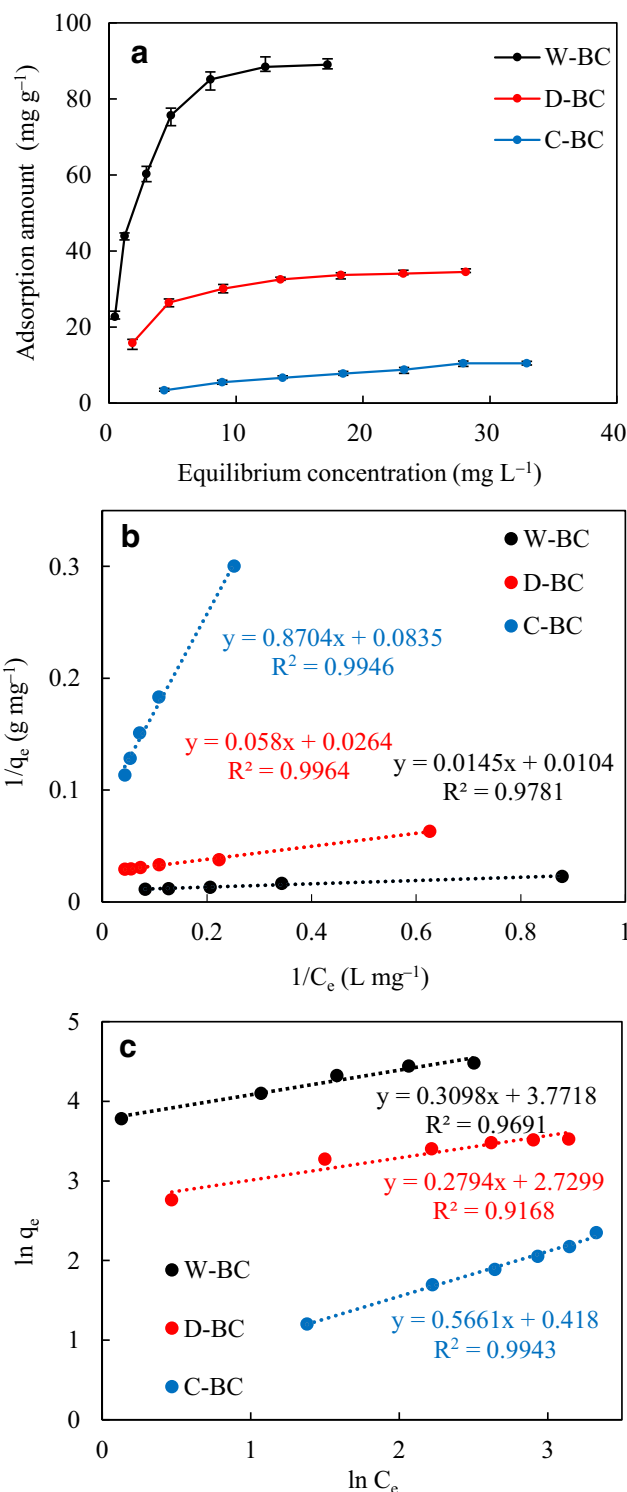
Fig. 4 **a** Adsorption capacity of MET on BCs (adsorbent dose = 0.20 g L^{-1}, at pH = 7.0 and 25 °C); **b** Langmuir linear models for MET on three BCs; and **c** Freundlich linear models for MET on three BCs (adsorbent dose = 0.20 g L^{-1}, at pH = 7.0 and 25 °C)

Therefore, the MET removal rate decreased for the BCs after recycling, and the decrease was most obvious with W-BC. However, the biomass used to produce the BC is derived from

Table 5 Maximum MET uptake capacity during adsorption of MET by various adsorbents

Adsorbent	Q_0 of MET (mg g^{-1})	Reference
Natural organic matter	3.90	Sigmund et al. 2019
Rice straw biochar	29.97	Ge et al. 2016
Medium microporous silicone	55.03	Zhao et al. 2021
Montmorillonite	84.75	Qu et al. 2020
W-BC	96.15	This study
D-BC	37.88	
C-BC	11.98	

cheap and abundant agricultural waste, so the amount of BC can be increased during recycling to obtain a greater removal effect.

Weight analysis based on correlations

As shown in Fig. 6a, in the MET adsorption process, the correlation coefficient for a specific BC was the most important parameter (46.11%), followed by C_0 for MET (19.29%). Excluding the ion concentration and contact time, the relative importance values for the other environmental parameters were all above 5%, thereby indicating that each environmental parameter had a great impact on the adsorption of MET. Similar results were obtained by Zhu et al. (2019) who calculated the correlations between various factors and the adsorption of pollutants by BC using the RF (random forest) model (Zhu et al. 2019). The amount of BC added and the pH were negatively correlated with the amount of MET adsorbed, and the correlation coefficients were determined as 14.83% and 11.90%, respectively. In order to increase the MET adsorption capacity in actual operations, the optimum amount should be added (0.20 g L^{-1} in this study) to maximize the adsorption effect of the BC. In addition, the adsorption environment should not be alkaline when using BC to adsorb MET. The physical characteristics and elemental compositions of the BCs had relatively strong correlations with the adsorption capacity, thereby indicating that the adsorption of MET by BCs involved both physical adsorption and chemical adsorption. The S_{BET} value, total pore volume, and average pore diameter all had relatively high correlation coefficients (7.77%, 7.73%, and 7.81%, respectively) with the adsorption capacity. Thus, when using BCs to adsorb MET in practice, BCs should be used with high S_{BET} values, low total pore volumes, and many micropores. In adsorption experiments, the atomic ratios of various elements are often used to characterize adsorbents. In particular, the atomic ratios of O/C and (N + O)/C represent the polarity of the adsorbent, where larger values indicate greater polarity. The H/C atomic ratio
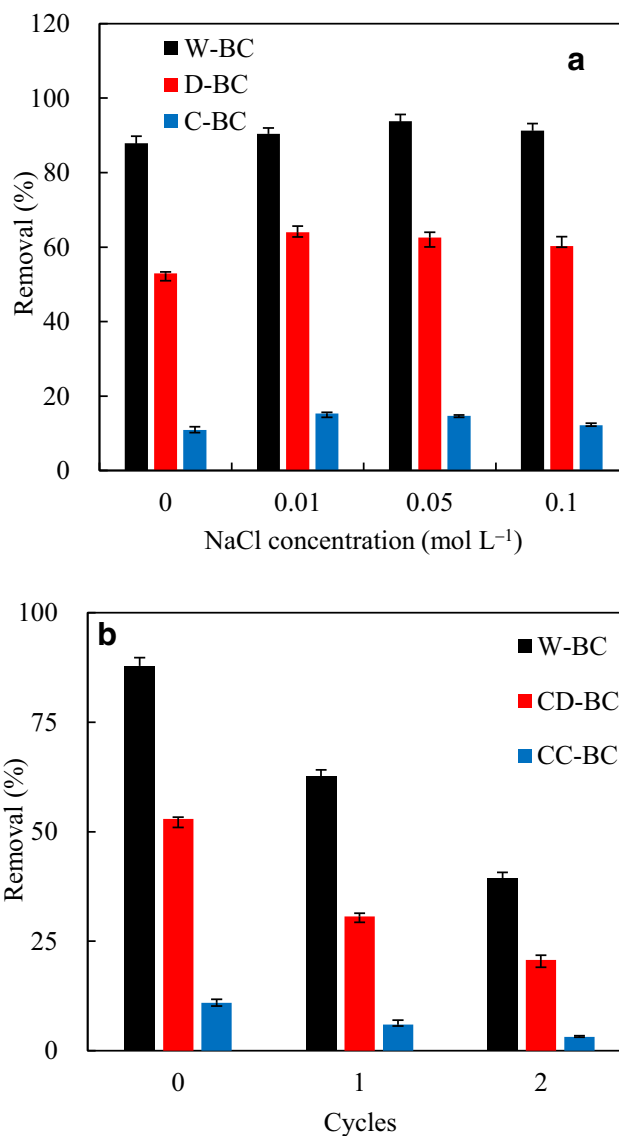
Fig. 5 **a** Effect of ionic strength on the adsorption of MET on three BCs (C_0 of MET (10.00 mg L^{-1}), adsorbent dose = 0.20 g L^{-1}, pH 7.0, at 25 °C); and **b** reusability of BCs (C_0 of MET (10.00 mg L^{-1}), adsorbent dose = 0.20 g L^{-1}, pH 7.0, at 25 °C)

represents the aromaticity of the adsorbent, where a smaller value indicates higher aromaticity (Chen and Chen 2009). According to the correlations determined with the O/C and (N + O)/C element ratios in our experiments, BCs with higher polarity are more suitable for the adsorption of MET. The results shown in Fig. 6a demonstrate that according to the MET adsorption tests, BCs with higher aromaticity are more affective at MET adsorption. As shown in Table 2, the H/C ratio was determined as less than 0.3 for W-BC, which indicates that W-BC formed a highly compact aromatize202d structure (Zhang et al. c). The (N + O)/C element ratio showed that a BC with greater polarity was more effective at MET adsorption. These correlations are shown in Fig. 6a. The characteristics of BCs are the most critical factors that affect the
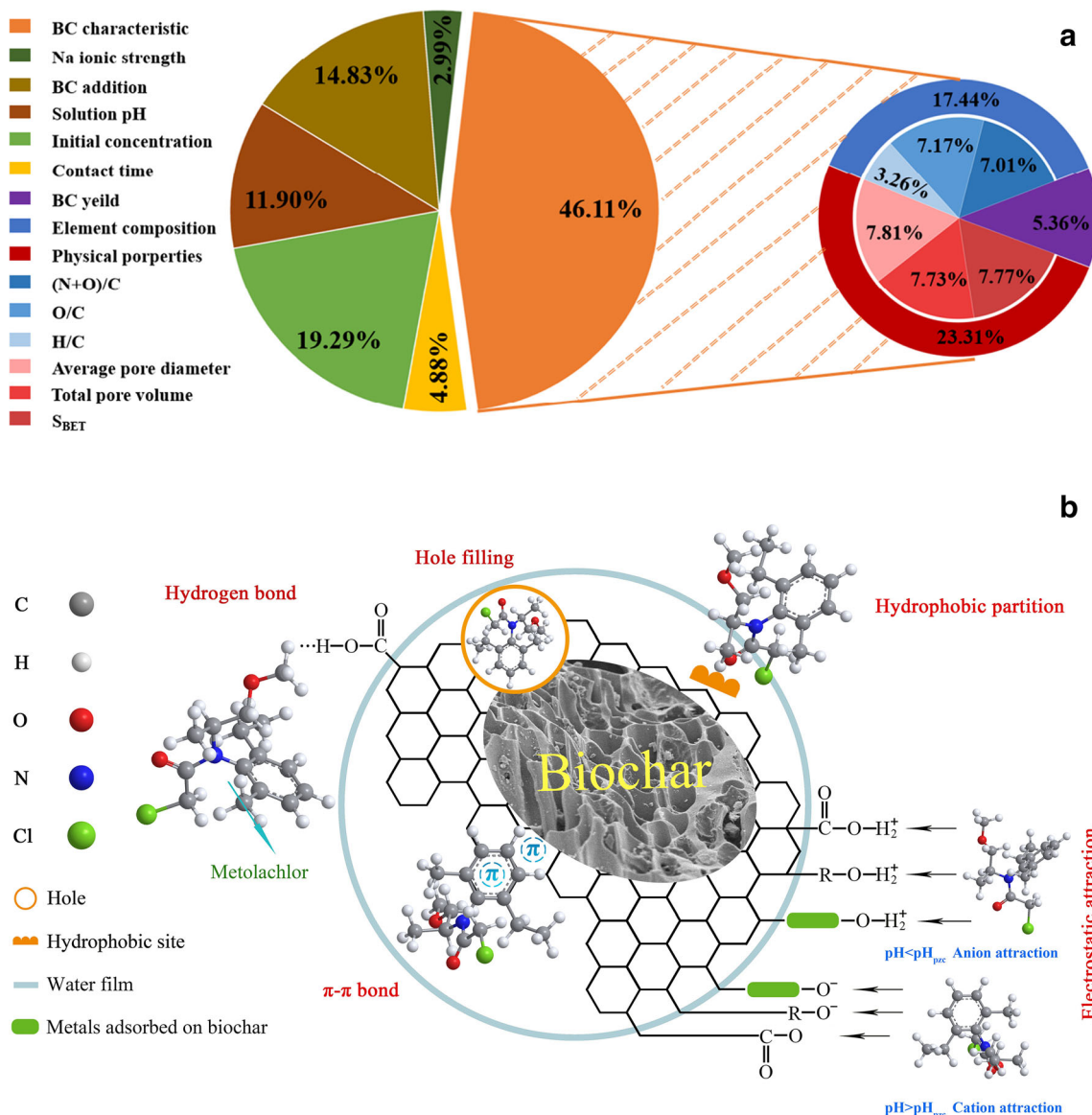
Fig. 6 **a** The contribution of each indicator to the adsorption capacity and **b** adsorption mechanism diagram

adsorption of MET. In particular, the S_{BET} value, pore volume, and pore diameter greatly influence the adsorption of MET by BCs. Thus, the findings obtained in this study confirm our hypothesis that the characteristics of BCs are the most important factors that affect the adsorption of MET.

Mechanisms responsible for MET removal by BCs

Figure 6b shows the mechanisms responsible for MET adsorption by BCs. The mechanisms associated with the adsorption of organic pollutants by BCs include physical adsorption, cation exchange, electrostatic adsorption, precipitation, and surface or inner spherical interactions (Dong 2018). Kinetic analysis showed that the adsorption of MET by BCs involved both physical and chemical adsorption processes. The physical adsorption process involved the adsorption interactions

between the adsorbent (BCs) and adsorbate (MET) via intermolecular attraction, such as the van der Waals force. Chemical adsorption involved hydrogen bonds, coordination bonds, and π–π bonds between the adsorbent and MET. The cracking process in BCs essentially involves the breaking of chemical bonds and the formation of new chemical bonds. As the cracking temperature increases, aliphatic hydrocarbon groups and hydroxyl groups on the surfaces of BCs are gradually converted into oxygen-containing functional groups such as carboxylic groups (Nie 2019). The surfaces of BCs are rich in oxygen-containing functional groups, which can promote the formation of hydrogen bonds between BC and organic pollutants with polar functional groups (Nie 2019). Our experimental pollutant adsorption results showed that the pore-filling effect was the main mechanism responsible for the adsorption of MET by BCs, where the pore-filling

effect is a microscopic adsorption mechanism. The strong adsorption of MET by microporous and mesoporous carbon is usually driven by specific interactions (Zhang et al. 2013). However, surface adsorption is only one of the mechanisms involved in the adsorption process. Our analysis of the ionization of MET in water showed that MET was weakly ionized in a highly acidic environment with a positive charge due to the electrostatic attraction to BC, thereby increasing the adsorption of MET. A partitioning effect also influenced the adsorption of MET, mainly due to the incomplete adsorption of MET by the carbonized components of BC in a linear adsorption process (Zhao et al. 2019). In summary, $\pi-\pi$ electron donor–acceptor interactions and hole filling may play dominant roles in the adsorption of MET by BCs, whereas electrostatic adsorption does not have a key role in the MET adsorption process.

Conclusions

In this study, walnut shells, cow dung, and corn cobs were sintered at high temperature to obtain BCs and used to remove MET from aqueous solution, and we investigated their adsorption performance. The results showed that the Q_0 values for MET adsorption by W-BC, D-BC, and C-BC were 96.15 mg g^{-1}, 37.88 mg g^{-1}, and 11.98 mg g^{-1}, respectively. W-BC had a significant adsorption effect and its adsorption capacity was high, where the adsorption equilibrium was reached in 30 min. The pore-filling effect, hydrogen bonds, and $\pi-\pi$ electron donor–acceptor phase were characterized as the main adsorption mechanisms. The adsorption environment greatly influenced the adsorption of MET, but the characteristics of the BCs mainly affected their adsorption performance. The adsorption of MET by BCs was better when they had a smaller average pore size, higher polarity, and greater aromaticity. The results showed that W-BC was an effective adsorbent with the advantages of simple and rapid MET removal from water. This method has high economic value due to the large amounts of MET residues in water and the lack of effective removal methods.

Declarations

Ethics approval This manuscript has not been published elsewhere and is not under consideration by another journal. We have approved the manuscript and agree with submission to ESPR. There are no conflicts of interest to declare.

Consent to participate and consent to publish All the authors contributed to the research and revision of this article, and mutually agree that it should be submitted to ESPR.

Competing interests The authors declare no competing interests.

References

Barra C, Giuliano G, Grenni P, Guzzella L, Pozzoni F, Bottoni P, Fava L, Crobe A (2005) Degradation and leaching of the herbicides metolachlor and diuron: a case study in an area of Northern Italy. Environ Pollut 103(3):525–534

Chen BL, Chen ZM (2009) Sorption of naphthalene and 1-naphthol by biochars of orange peels with different pyrolytic temperatures. Chemosphere 76(1):127–133

Chen Y, Zhang X, Chen W, Yang H, Chen H (2017) The structure evolution of biochar from biomass pyrolysis and its correlation with gas pollutant adsorption performance. Bioresour Technol 246:101–109

Cwielag-Piasecka I, Medynska-Juraszek A, Jerzykiewicz M, Debicka M, Bekier J, Jamroz E, Kawalko D (2018) Humic acid and biochar as specific sorbents of pesticides. J Soils Sediments 18(8):2692–2702

Dai Y, Zhang K, Meng X, Li J, Guan X, Sun Q, Sun Y, Wang Y, Wang W (2019a) New use for spent coffee ground as an adsorbent for tetracycline removal in water. Chemosphere 215:163–172

Dai Y, Zhang N, Xing C, Cui Q, Sun Q (2019b) The adsorption, regeneration and engineering applications of biochar for removal organic pollutants: a review. Chemosphere 223:12–27

Dai Y, Li J, Shan D (2020) Adsorption of tetracycline in aqueous solution by biochar derived from waste Auricularia auricula dregs. Chemosphere 238:124432

Deng X, Zheng W, Zhan Q, Deng Y, Zhou Y, Bai L (2020) New lead discovery of herbicide safener for metolachlor based on a scaffold-hopping strategy. Molecules 25(21):4986

Dong C (2018) Effects of biochar and its aging on the adsorption mechanism of cadmium and ammonia nitrogen, Ph.D. Dissertation, Wuhan University

Ge C, Guo X, Li J, Lv J, Liu S, Xu H (2016) Adsorption and slow-release effect of rice straw biochar on metolachlor. J Ecology Rural Environ 132(01):168–172

Guelfi D, Gozzi F, Machulek A, Sires I, Brillas E, de Oliveira S (2018) Degradation of herbicide S-metolachlor by electrochemical AOPs using a boron-doped diamond anode. Catal Today 313:182–188

He X, Jiang J, Hong Z, Pan X, Dong Y, Xu R (2020) Effect of aluminum modification of rice straw-based biochar on arsenate adsorption. J Soils Sediments 20(8):3073–3082

Hu J (2009) Study on the immunotoxic effect of metolachlor in mice. J Harbin Med Univ 1:57–59

Josef V, Alzbeta S, Eliska Z, Jan K, Milos B, Antonin K (2018) Chronic toxicity of metolachlor oa on growth, ontogenetic development, antioxidant biomarkers and histopathology of early life stages of marbled crayfish. Sci Total Environ 43:1456–1463

Kan T, Strezov V, Evans TJ (2016) Lignocellulosic biomass pyrolysis: a review of product properties and effects of pyrolysis parameters. Renew Sust Energ Rev 57:1126–1140

Kumar Y, Singh N, Singh S (2017) Removal of herbicides mixture of atrazine, metribuzin, metolachlor and alachlor from water using granular carbon. Indian J Chem Technol 24(4):400–404

Li C, Zhang L, Gao Y, Li A (2018) Facile synthesis of nano ZnO/ZnS modified biochar by directly pyrolyzing. Waste Manag 79:625–637

Liu C, Chen L, Ding D, Cai T (2019) From rice straw to magnetically recoverable nitrogen doped biochar: efficient activation of peroxymonosulfate for the degradation of metolachlor. Appl Catal B-environ 254:312–320

Mandal A, Singh N, Purakayastha T (2017) Characterization of pesticide sorption behaviour of slow pyrolysis biochars as low cost adsorbent for atrazine and imidacloprid removal. Sci Total Environ 577:376–385

Nguyen T, Xu C, Tahmasbian I, Che R, Xu Z, Zhou X, Wallace H, Bai S (2017) Effects of biochar on soil available inorganic nitrogen: a review and meta-analysis. Geoderma 288:79–96

Nie T (2019) Effect of aging on the adsorption of tetracycline and copper on biochar and mechanism research. Ph.M. Dissertation, Zhejiang University

Orge C, Pereira F, Faria J (2017) Photocatalyic-assisted ozone degradation of metolachlor aqueous solution. Chem Eng J 318:247–253

Otero R, Fernandez J, Ulibarri M, Celie R, Bruna F (2016a) Adsorption of non-ionic pesticide S-Metolachlor on layered double hydroxides intercalated with dodecylsulfate and tetradecanedioate anions. Appl Clay Sci 65:72–79

Otero R, Lopez M, Esquivel D, Fernandez J (2016b) Romero-Salguero, F., Removal of S-metolachlor herbicide from aqueous solutions by meso and microporous organosilica materials. Microporous Mesoporous Mater 278:35–43

Ozcimen D, Ersoy-Mericboyu A (2010) Characterization of biochar and bio-oil samples obtained from carbonization of various biomass materials. Renew Energy 35(06):1319–1324

Qu JH, Akindolie MS, Feng Y, Jiang Z, Zhang GS, Jiang Q, Deng FX, Cao B, Zhang Y (2020) One-pot hydrothermal synthesis of NaLa(CO3)(2) decorated magnetic biochar for efficient phosphate removal from water: Kinetics, isotherms, thermodynamics, mechanisms and reusability exploration. Chem Eng J 394:124915

Rode J (2019) Statistical software output in the classroom: a comparison of R and SPSS. Teach Psychol 46(4):319–327

Rose C, Coupe R, Capel P, Webb R (2018) Holistic assessment of occurrence and fate of metolachlor within environmental compartments of agricultural watersheds. Sci Total Environ 612(15):708–719

Rytow G, Gonen Y, Afuta S (2008) Preparation of berberine-montmorillonite-metolachlor formulations from hydrophobic/hydrophilic mixtures. Appl Clay Sci 41:47–60

Shattar S, Zalzaria N, Foo K (2019) Preparation of a montmorillonite-derived adsorbent for the practical treatment of ionic and nonionic pesticides. J Mater Res Technol 8(5):4713–4724

Sigmund G, Castan S, Wabnitz C, Bakkour R, Huffffer T, Hofmann T, Elsner M (2019) NO2 and natural organic matter affect both soot aggregation behavior and sorption of S-metolachlor. Environ. Sci.: Proc. Imp. c9em00354a

Stapf D (2017) Efficiency of biomass energy: an exergy approach to biofuels, power and biorefineries. Chem Ing Techol 89(6):831–838

Sun Y, Zhao L, Li X, Hao Y, Xu H, Weng L, Li Y (2019) Stimulation of earthworms (Eisenia fetida) on soil microbial communities to promote metolachlor degradation. Environ Pollut 248:219–228

Szabo N (2015) Hydraulic conductivity explored by factor analysis of borehole geophysical data. Hydrogeol J 23(5):869–882

Tijani H, Yuzir A, Abdullah N, Sallis P (2017) Impact of (RS)-MCPP herbicide and sulphate on the treatment performance, kinetics and microbial diversity of anaerobic membrane bioreactor. J Environ Eng 5(6):5389–5395

Treviño-Cordero H, Juárez-Aguilar L, Mendoza-Castillo D, Ernández-Montoya V, Montes-Morán M (2013) Synthesis and adsorption properties of activated carbons from biomass of Prunus domestica and Jacaranda mimosifolia for the removal of heavy metals and dyes from water. Ind Crop Prod 42:315–323

Vinhal J, Lima C, Cassella R (2016) Sorption of the herbicides diquat and difenzoquat from aqueous medium by polymeric resins in the presence of sodium dodecylsulfate: kinetic and mechanistic study. J Environ Sci Health B 51(7):482–489

Wei L, Huang Y, Li Y, Huang L, Mar N, Huang Q, Liu Z (2016) Biochar characteristics produced from rice husks and their sorption properties for the acetanilide herbicide metolachlor. Environ Sci Pollut R 24(5):4552–4562

Wei S, Zhu M, Song J, Peng P (2017) Comprehensive characterization of biochars produced from three major crop straws of China. Bioresources 12(02):3316–3330

Wu C, Shemer H, Linden K (2007) Photodegradation of metolachlor applying UV and UV/H2O2. J Agric Food Chem 55(10):4059–4065

Xu J, Zhang D, Nie M, Wang H, Li L (2020) Adsorption of Cr6+ on polyethyleneimine-functionalized straw biochar from aqueous solution. Chem J Chinese U 41(1):155–161

Yang Y, Lin X, Wei B, Zhao Y, Wang J (2014) Evaluation of adsorption potential of bamboo biochar for metal-complex dye: equilibrium, kinetics and artificial neural network modeling. Int J Environ Sci Technol 11(4):1093–1100

Yu L, Pan Y, Wu Y (2009) Research on standardized methods of comprehensive evaluation data of academic journals. J Books and information work 53(12):136–139

Yuan S, Zhao L, Meng H, Shen Y (2016) The main types, physical and chemical properties and research prospects of biochar. Plant Nutr Fert Sci 22(5):1402–1417

Zhang P, Sun H, Yu L, Sun T (2013) Adsorption and catalytic hydrolysis of carbaryl and atrazine on pig manure-derived biochars: impact of structural properties of biochars. J Hazard Mater 244:217–224

Zhang P, Li Y, Cao Y, Han L (2019) Characteristics of tetracycline adsorption by cow manure biochar prepared at different pyrolysis temperatures. Bioresour Technol 285:121348

Zhang W, Du W, Wang F, Xu H, Zhao T, Zhang H, Ding Y, Zhu W (2020) Comparative study on Pb2+ removal from aqueous solutions using biochars derived from cow manure and its vermicompost. Sci Total Environ 716:137108

Zhang Y, Akindolie MS, Tian X, Wu B, Hu Q, Jiang Z, Wang L, Tao Y, Cao B, Qu JH (2021) Enhanced phosphate scavenging with effective recovery by magnetic porous biochar supported La(OH)3: Kinetics, isotherms, mechanisms and applications for water and real wastewater. Bioresource Technol 319:124232

Zhao Z, Wu Q, Nie T, Zhou W (2019) Quantitative evaluation of relationships between adsorption and partition of atrazine in biochar-amended soil with biochar characteristics. RSC Adv 9(8):4162–4171

Zhao J, Gao F, Sun Y, Fang W, Li X, Dai Y (2021) New use for biochar derived from bovine manure for tetracycline removal. J Environ Chem Eng (In Press)

Zhong B, Wang S, Dong H, Luo Y, Jia Z, Zhou X, Chen M, Xie D, Jia J (2017) Halloysite tubes as nanocontainers for herbicide and its controlled release in biodegradable poly(vinyl alcohol)/starch film. J Agric Food Chem 65(48):10445–10451

Zhu X, Wang X, Ok Y (2019) The application of machine learning methods for prediction of metal sorption onto biochars. J Hazard Mater 328:4–13